RESEARCH ARTICLE

Macromolecular Materials and Engineering
www.mame-journal.de

Micro- and Nanotexturization of Liquid Silicone Rubber Surfaces by Injection Molding Using Hybrid Polymer Inlays

Nekane Lozano-Hernández, Germán Pérez Llanos, Carlos Saez Comet, Luis J. del Valle,* Jordi Puiggali, and Enric Fontdecaba*

Micro- and nanotexturization of surfaces can give to the parts different advanced functionalities, such as superhydrophobicity, self-cleaning, or antibacterial capabilities. These advanced properties in combination with the biocompatibility of Liquid Silicone Rubber are an interesting approach for obtaining high-performance medical devices. The industrial production of surface textures in polymeric materials is through the replication technique, and the best option to attain a high production rate is injection molding. Moreover, its low viscosity during processing can provide an accurate replication capacity by the easy filling by capillarity of the microtextures. An innovative replicating technique for Liquid Silicone Rubber is presented by studying the replication of different shaped textures within a diameter range of between 2 and 50 µm. The copying process consists in the overmolding of a textured polymeric inlay obtained by nanoimprint lithography. At the end of the process, a textured part is obtained, while the imprinted film remains in the mold. The injection molding parameters are optimized to increase the replication accuracy, and their effect on texture replicability is analyzed and discussed. Finally, it is shown that the textured surfaces improve their wettability behavior, which is a necessary and important characteristic in the development of biomedical devices.

1. Introduction

Surface textures are characteristics of nature that obey the adaptation of organisms to different environmental conditions. This adaptability is a source of inspiration to the scientific community, which has models of surface replication in textured plant cuticles or animal skins.[1] Surface textures may provide interesting properties such as self-cleaning capacity, superhydrophobicity,[2–4] dry adhesion,[5] friction reduction,[6,7] or structural colors.[8] Thus, surface texturization offers a combination of engineering properties that can be exploited in many applications. Therefore, several attempts are currently being made to replicate natural textures in metals and polymers.[9]

Exploring the possibilities of replication in materials, Liquid Silicone Rubber (LSR) appears as a good candidate to evaluate the replication of microtextures. This material is of great interest to the medical industry due to its biocompatibility.[10,11] These medical applications have interesting synergies with surface texturing, since pieces with antibacterial properties,[12] cell alignment,[13,14] and high wettability[15] can be obtained. Therefore, it is interesting to investigate methods that allow the mass production of the pieces with surface textures. In previous works, different replication techniques were reported. In such procedures, the replication processes are not direct methods since they require a first step to produce the LSR part and then a second step for the specific surface treatment (laser,[9,16] chemical,[14,17] plasma treatment[18]). Moreover, while the surfaces show non-regular textures, these techniques have a low productivity rate compared to other texturing methods. Thus, several replication processes have been postulated to achieve nanotextures during the whole manufacturing process of an LSR part. Some relevant methods directly place the silicone in the textured mold[19,20] or injection molding with a textured insert.[21,22] These replication methods need a patterned metallic mold, designed according to the targeted textures, to be used as a template. An alternative manufacturing method to increase the manufacturing cadence is injection molding. It also allows a higher surface resolution to be obtained than placing the material over the mold without any pressure. Despite the accurate replication obtained with metallic inserts, the marked difference in hardness between the mold and the counterparts may give rise to some problems, such

N. Lozano-Hernández, G. Pérez Llanos, C. Saez Comet, L. J. del Valle, J. Puiggali
Departament d'Enginyeria Química
Universitat Politècnica de Catalunya (UPC)
C/ Eduard Maristany 10–14, Barcelona 08019, Spain
E-mail: Nekane.lozano@eurecat.org; Luis.javier.del.valle@upc.edu

N. Lozano-Hernández, G. Pérez Llanos, C. Saez Comet, E. Fontdecaba
Eurecat, Centre Tecnològic de Catalunya
Unit of Polymeric Materials and Processes
Av. Universitat Autònoma, 23, Cerdanyola del Vallés 08290, Spain

J. Puiggali
Institute for Bioengineering of Catalonia (IBEC)
The Barcelona Institute of Science and Technology (BIST)
Carrer Baldiri i Reixac 11–15, Barcelona 08028, Spain

The ORCID identification number(s) for the author(s) of this article can be found under https://doi.org/10.1002/mame.202100741

DOI: 10.1002/mame.202100741

as the breakage of the copied microtextures during demolding.[21] Aimed at overcoming such problems, one possibility is to use a material in the mold with similar elastic properties to the counterpart. In this sense, the use of textured polymeric films is presented as a good alternative, as it has been reported in the injection of thermoplastics.[23,24] The flexible templates can be adapted for their use in LSR injection. A metallic master stamp is used to obtain the flexible polymeric inserts by Nanoimprint Lithography (NIL).[25,26] Each flexible film can be employed for several injection cycles, and in this way, the life of the metallic stamp can be extended, since it is used only one time for each film. Moreover, the polymeric inlays attached to the mold have a temperature isolating capability, which retards the vulcanization process at the surface. This means that the polymer has high fluidity for longer times, which helps the proper filling by capillarity of all surface micro- and nanotextures.[21] Other techniques can be useful for the obtention of polymeric textured films and metallic molds (e.g., Direct Laser Interface Pattering (DLIC)). Previous work can be addressed that study this technique in metallic molds and thermoplastic films with accurate results.[27,28] To our knowledge, few works that study the replication of microtextures by injection molding[21,22] have addressed the use of LSR.

This work aims to study the replication of microtextures in LSR pieces in mass by injection molding. Polymeric films were adapted to the injection of LSR and used as templates. Microtextures with different geometries and dimensions were generated and analyzed. Optimizing the injection parameters can improve the replication of microtextures for different geometries and at different textured region locations. Wettability and mechanical behavior were evaluated for the different microtextured parts to assess the effect of the microfeatures.

2. Experimental Section

2.1. Manufacture of Polymeric Stamps

The material used as a substrate is a polyetherimide (PEI), Ultem 1000B (Sabic), of 75 µm thickness. This material was chosen due to its heat deflection temperature (190°C). PEI films were covered with Ormostamp (from Microresist Technology), a UV curing organic-inorganic hybrid polymer with thermal stability up to 270°C. This resin was commonly employed in a previous UV-NIL replication work.[29]

NIL technology provided the silicon masters containing the microtextures. Both masters were manufactured by electron beam lithography, a technique based on the definition of features by a focused, energetic beam of electrons on a resist.[30] Two different silicon molds were used: micro and sub-micro standard stamps. Both consist of squares with dimensions of 20×20 mm and textured areas with different diameters and geometries. The micro standard stamp contained four different patterns (vertical and horizontal lines, pillars, and holes) of four different dimensions (1, 5, 10, and 50 µm) arranged in small squares of 4×4 mm. In all cases, the height of the indicated microfeatures was 2 µm. The sub-micro master stamp contained 5×5 mm squares constituted by vertical lines, pillars, and holes of 0.5, 1.0, and 2.0 µm. The height of the microfeatures was 1 µm (**Figure 1**a). Figure 1b,c shows electron microscope images of two representative textures. This variety of textures has been chosen

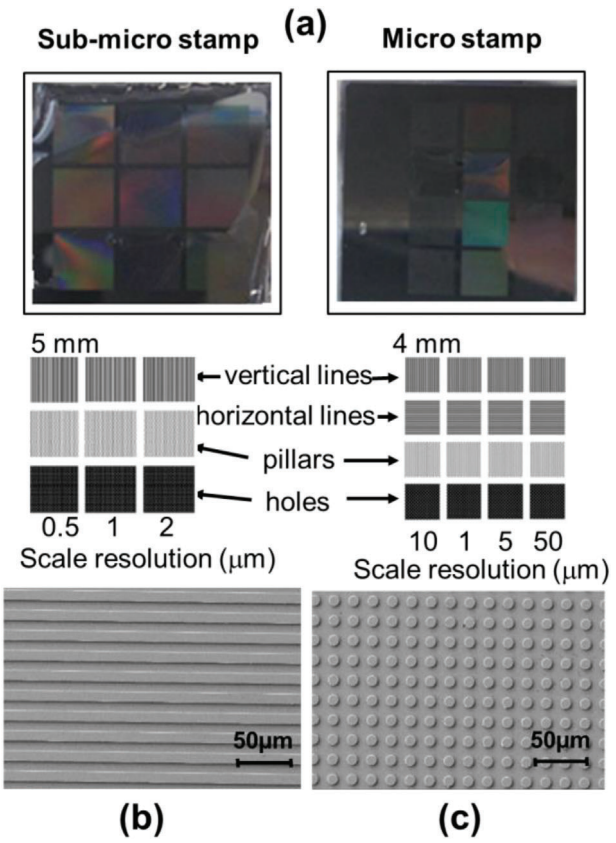

Figure 1. a) Images of the silicon master stamps with the disposition and diameters. b) SEM image of 10 µm lines in the silicon master stamp. c) SEM image of 10 µm pillars in the silicon master stamp.

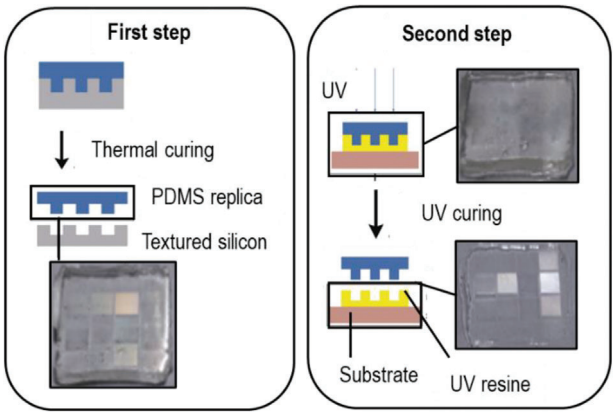

Figure 2. Schematic representation of the surface texturization: first, the production of the PDMS negative replica by thermal NIL and second the UV NIL replication on plastic foils with real images of each part.

to obtain information on replication in lateral dimensions of different orders of magnitude and different aspect ratios. Previous publications worked on the replication of pillars,[21,22] so in this work, the viability of replicating other geometries is analyzed.

The replication consists of a two-step process (**Figure 2**). In the first step, a polydimethylsiloxane (PDMS) negative replica from the silicon stamps was obtained. PDMS (Sylgard 184 from

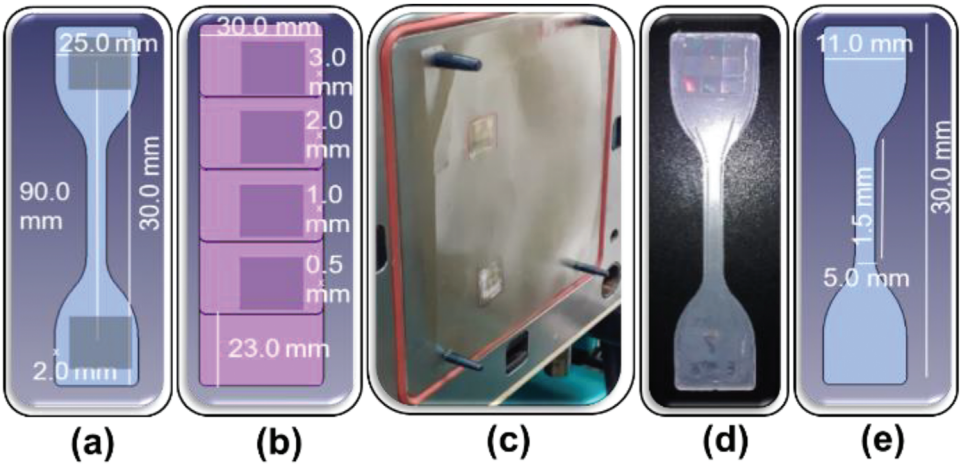

Figure 3. a) The 2D mold of dumbbell geometry and measurements. b) The 2D mold of stairs geometry and measurements. c) Textured film for the dumbbell geometry fixed into the mold. d) Textured LSR dumbbell part with the textured areas matching the textures printed on the films. e) Dimensions of the dumbbell geometry for the tensile test.

Table 1. Technical parameters of Elastosil LR3003/70A/B.

Property	Value	Method
Viscosity, dynamic (1 s^{-1})	1 200 000 mPa s	DIN EN ISO 3219
Viscosity, dynamic (10 s^{-1})	400 000 mPa s	DIN EN ISO 3219
Hardness Shore A	70	DIN ISO 7619-1
Tensile strength	8.6 N mm^{-2}	ISO 37 type 1
Elongation at break	290%	ISO 37 type 1
Compression Set	12%	DIN ISO 815-1 type B method A

Dow Corning) is a heat-curable silicone presented in two different components: a base (prepolymer) and a curing agent (crosslinker) useful for replication on sub-micron resolution. Both components are mixed in the ratio 1:10 and deposited over the silicon stamp.[31] After a curation process in an oven for 10 min at 150 °C, a PDMS negative replica was obtained. For the second step, PEI was used as substrate. The surfaces of PEI were cleaned and treated with O_2 plasma to improve their adhesion. A 50 µm of Ormostamp coating was deposited over the substrate. The second step consists of texturing the UV resin using the PDMS replica as a template. Thus, the film is exposed to UV light of wavelength 315–395 nm for 1 min, at an intensity of 90 W cm^{-2}. After curing, the PDMS replica is peeled off of the film, which is valid for the injection process.

2.2. Injection Molding

Elastosil LR3003/70A/B from Wacker (see technical parameters in **Table 1**) was injected using an Arburg Allrounder S 500-170 machine. The injection molding process started with the two separated components of LSR. A 2KM Silcostar 902 dosing system pumped both components from the pails and mixed them with a static mixer. The injection unit was cooled, and the material was injected into a hot mold where the chemical reaction of vulcanization took place. The mold used has two different geometries, which allow the influence of different parameters of the specimen to be studied (**Figure 3**a,b, the grey zones correspond to the positions of the textured regions). In the case of the dumbbell geometry (Figure 3a), two textured areas were placed in the wide parts of the figure, separated by ≈9 cm. The injected LSR enters the mold from the top. It is possible to evaluate the difference in replication with the distance to the injection point comparing the replication of the "up" and "down" textured regions (Section 3.1). On the other hand, the geometry of the stairs (Figure 3b) is interesting for evaluating the replication in different thicknesses (Section 3.2). Textured regions were placed in each stair with thicknesses of 3.0, 2.0, 1.0, and 0.5 mm. To fix the texturized film to the mold, a hole was made in each corner of the film, and then the holes were fitted over four pins in the mold (Figure 3c). The holes in the film and the pins in the mold are designed to ensure accurate positioning of the textured regions in the figure. A picture of a final textured dumbbell part after the injection process is shown in Figure 3d.

The optimization of the injection molding parameters allowed the replication grade to be increased. The main injection parameters that were first studied were curing time (t_c), mold temperature (T_m), and injection speed (vs). An in-depth study of the replication accuracy obtained for different processing conditions has been carried out to define the process window. In the process window, both the good replication of the textures and the good filling of the pieces have been taken into account. For this reason, an adjustment is made in each of the sections that involve a change in the geometry of the mold. The proposed mold temperature range was above the recommended operating temperature to ensure enough mechanical resistance of the textured films for performing the tests. Specifically, optimization was carried out in the 130–160 °C, 30–60 s and 10–50 cm^3 s^{-1} intervals for T_m, t_c and v_i, respectively. The curing times and mold temperatures used have been proven to provide good curing of the part. The parameters used in each test and geometry will be specified in the results.

Finally, the textured silicone was washed in ethanol and dried at room temperature before characterizing its textured surface.

2.3. Topology and Texture Characterization

Surface textures were characterized using confocal microscopy. The images were obtained with a confocal laser scanning microscope (LSM 900 Zeiss) controlled by ZEN 2.6 software (blue edition) (Carl-Zeiss Microscopy GmbH, Jena, Germany).

Measurements of heights, widths, profiles and 3D images were obtained for the parts of each parameter set. A degree of transcription parameter (*DOT*) was used to evaluate and compare the replication of each texture. *DOT* is defined as the ratio between the height of the features in the silicon master stamp (h_m) and the filling depth (h_f)) in the LSR parts:[11]

$$DOT = \frac{h_f}{h_m} \tag{1}$$

Three different parts at three distinct zones of each texture were evaluated to determine the *DOT* values, and the results were averaged. The *DOT* obtained values are represented in a histogram considering the confidence interval of 95%. The middle point of the normal fitting is the average *DOT* value, and the width of the distribution is the standard deviation. The magnification objective and the scanned area were adapted for each feature and diameter. To analyze the results, the focus of attention was placed on textures above 2.0 µm; for 0.5 and 1.0 µm. The state of the original silicon master stamp was not optimum, and a large dispersion was found in replication.

Surface roughness parameters were calculated from the confocal images using the software Gwyddion v2.60 (http://gwyddion.net/).

SEM micrographs of the silicon master stamps were taken with a Focused Ion Beam Zeiss Neon40 microscope (Zeiss, Oberkochen, Germany) operating at 5 kV. Silicon stamps were mounted on an aluminum pin-stub using a double-sided adhesive carbon disc (Ted Pella Inc., Redding, CA, USA). Silicone textured samples have been coated with carbon before observing at the SEM.

2.4. Contact Angle Measurements

Contact angles (θ_c) were measured at room temperature with sessile drops using an OCA-15 plus Contact Angle Microscope (Data-Physics Instruments GmbH, Filderstadt, Germany) and SCA20 software (Version 2.0, Data-Physics Instruments GmbH, Filderstadt, Germany). Contact angle values of the right and left sides of deionized water drops were measured at a constant temperature of 20 °C and averaged. Measurements were performed 2 s after the drop (5 µL) was deposited on the sample surface. All θ_c data was an average of six measurements on different surface locations.

2.5. Mechanical Properties and Degree of Crosslinking

The stress-strain curves have been determined from a Zwickroell BT1-FR050TH.A1K, with a maximum force of 50 kN. The tensile test was measured for dumbbell-shaped test specimens (dimensions on Figure 3e) obtained by cutting each thickness of the geometry of the stairs (Figure 3b). The strain rate is 50 mm s^{-1} for all the thicknesses.

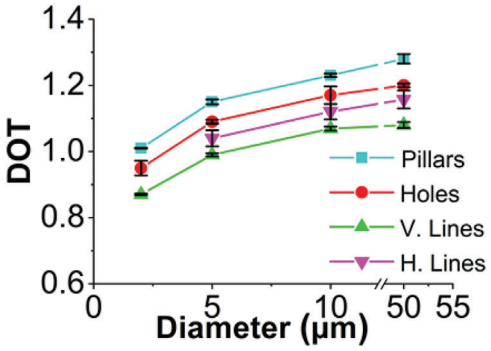

Figure 4. Comparison of *DOT* (relation between the height of replication and the height of the master) obtained for all the diameters (or lateral dimensions in the case of lines) for all the available textures.

The number of crosslinks per unit volume (n) in LSR is related to the elastic modulus (E) by[32]

$$n = \frac{E}{3RT} \tag{2}$$

where R is the universal gas constant ($R = 8.31$ J K^{-1} mol^{-1}) and T the test temperature (room temperature, i.e., 293 K). E is the elastic modulus obtained from the tensile curve as the slope of the elastic regime.[33]

3. Results and Discussion

3.1. Dependence of Replication on the Distance to the Injection Point

Figure 4 shows the *DOT* (Degree of Transcription) values for the replication of the textures in the top position of the dumbbell for the fixed injection parameters ($T_m = 135$ °C, $t_c = 60$ s, $v_i = 30$ cm^3 s^{-1}). These experimental results show that DOT is higher than 1 for most of the obtained textures. It indicates that the structures on the replica were taller than those present in the master stamp. It is important to note that some stretching of textures occurred when parts were removed from the mold. This effect is similar to the reported stretching in themoplastic nanopillars,[23] but in this case the observation was extended to the different geometries and diameters. Comparing the geometries, the stretch was more pronounced in the case of pillars and holes than in lines. The contact area between the structure and the negative replica in the film was higher for these two geometries, and a higher frictional force is expected during the demolding step. Moreover, the stretch was also different for vertical and horizontal lines, the latter having a slightly higher DOT value. This feature seems to be caused by a difference in stretch due to the direction of the demolding process, rather than a preferential filling due to the orientation of the lines. The stretch supported by the different textures also had a dependence on the diameter/dimensions of the microfeatures. Specifically, it was observed that stretching increased with dimensions independently of the considered geometry. This experimental observation can be explained considering that the volume of material involved in the microfeatures increases with larger dimensions. Nevertheless, the stretching, and therefore the DOT,

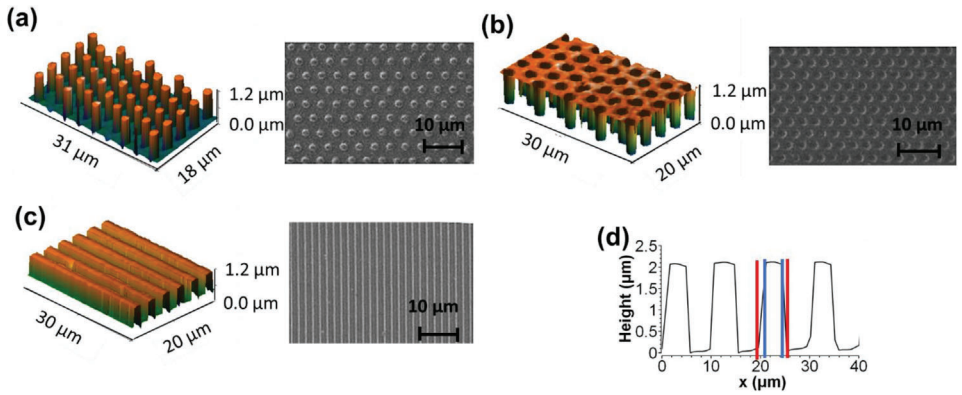

Figure 5. Images of well-replicated a) pillars, b) holes and c) lines of 2 µm. On the left of each image appears a confocal 3D reconstruction and, on the right, its respective SEM image. d) Plot showing the height profiles of 5 µm pillars in the *x*-direction (following the width of the stair) (d). The width between red lines is 5.04 µm and between blue lines is 4.23 µm.

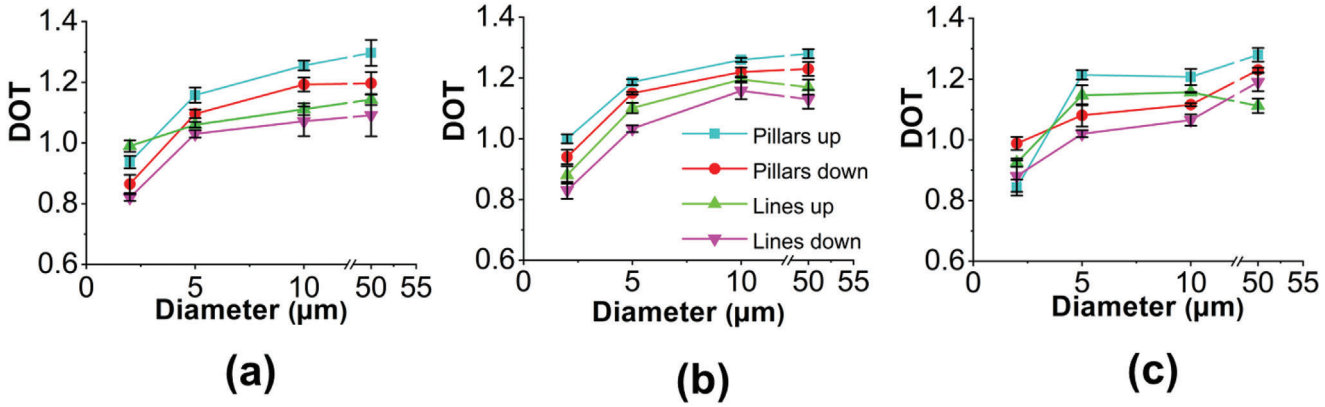

Figure 6. *DOT* values (relation between the height of replication and the height of the master) represented for each diameter (lateral dimensions in the case of horizontal lines) in the top and bottom regions of the dumbbell specimen for different injection speeds: a) 30 cm^3 s^{-1}, b) 40 cm^3 s^{-1}, and c) 50 cm^3 s^{-1}. Symbols of the legend are represented in figure (b).

tends to be stabilized when dimensions reach a value close to 10 µm. The obtained results allow the analysis of the injection results for dumbbell and stairs geometries to be reduced to only the pillar and the vertical line textures, since orientation does not influence the replication, and the behavior of the hole texture was not distinctive.

The low standard deviation in the determination of DOT in every texture, as well as the 3D confocal and SEM images of the different 2 µm textured surfaces (**Figure 5**a–c) processed under optimal conditions, indicate that replicated features were highly homogeneous in height. In addition, the use of polymeric films avoid the breakage of the microtextures during demolding, comparing to the rupture that take place in the replication using metallic textured molds reported in previous works.[21,22] Figure 5d illustrates the deformation of pillars caused by stretching. Note that the diameter on the base of the pillars is significantly higher than that on the top, resulting in a trapeze shape.

Concerning the replication dependence on the distance to the injection point, **Figure 6** shows the *DOT* values for "up" (i.e., near the injection point) and "down" (i.e., 9 cm away from the injection point) positions. The parameters used in this comparison are those that have given the best part filling result and replication. Temperature and curing time remain constant (T_m = 135 °C, t_c = 60 s). It can be seen that the geometry of the texture differs slightly in the replication, the results being practically independent of the specific shape of the microfeatures (e.g., pillars and horizontal lines, Figure 4). These slight differences in the replication depending on the zone of the part was also reported in previous works.[22] To better understand the effect of this replication changes depending on the location, different injection speed were analyzed. Slight differences in replication were found considering the injection speed: i) Replication was better in the region close to the injection point when the speed was 30 cm^3 s^{-1} (Figure 6a). The lower velocity gives rise to a lower friction rate of the silicone over the film at the entrance. Therefore, a more progressive filling of microstructures in this region was obtained. In addition, textures located at a greater distance from the injection point are filled with higher difficulty when the injection velocity decreases and the viscosity increases (i.e., 2 µm textures). ii) At medium speed, replication differences between the up and down regions were negligible, and only a slight difference was detected, depending on the geometry (Figure 6b). iii) Almost

Table 2. Representative parameter sets considered in the replication study from the stairs mold geometry.

Parameter set	Mould temperature T_m [°C]	Injection speed v_i [cm^3 s^{-1}]	Curing time t_c [s]
S_1	150	15	30
S_2	150	50	30
S_3	135	30	60
S_4	135	50	60

no differences in the replication were observed for the highest speed (i.e., 50 cm^3 s^{-1}) considering both position and geometry (Figure 6c). Performed tests revealed again that pillars present a greater stretch than lines in the different positions and velocities.

3.2. Dependence of Replication with the Thickness of the Parts

As shown throughout the section, the four-parameter sets summarized in **Table 2** have been modified to improve replication accuracy.

Non-accurate replication was observed for parts with a thickness equal to or lower than 2 mm when the highest mold temperature was employed, independently of the injection speed and even of the curing time (i.e., parameter sets S_1 and S_2). The main explanation is that the LSR decreases its viscosity at this temperature due to premature vulcanization of the silicone. This change in fluidity does not allow the microtextures mold to fill properly. Specifically, **Figure 7**a shows the comparison between height profiles obtained from the first two stairs using the parameter set S_1 (i.e., T_m of 150 °C). The textures appeared highly deformed for the stair with 2 mm thickness, as seen in the 3D image given in Figure 7b. Pillar replication was, indeed, barely detected for the successive lower thicknesses, and basically only a periodic roughness was detected on the surface of the injected specimens. The loss in replication was also independent of texture diameter.

The results obtained for parameters set S_2 were similar to those obtained for S_1, despite increasing the injection speed. Nevertheless, replication results were good enough for stair number 2 with a 2 mm thickness. The increase in injection speed allows premature vulcanization to be delayed, making it possible to fill this second step.

Despite this, the replication for 1 mm has low accuracy. **Figure 8**a,b shows the effect of the thickness of the injected specimens on the loss of the shape of microfeatures. Pillar and line textures displayed similar behavior with a loss of shape in profiles (Figure 8a,b) when thickness decreased from 2 to 1 mm. Height profiles showed that deformation began at the 2 mm stair, and was more marked at the 1 mm stair. Behavior in the case of lines and pillars was similar. Results were similar for textures independently of the size/diameter of microfeatures.

Aimed at improving the replication results for the lower thickness, the working temperature was lowered to maintain the injected material with greater fluidity. The injection speed was kept high to avoid the effect of the distance to the injection point (see parameter sets S_3 and S_4). The curing time was increased to

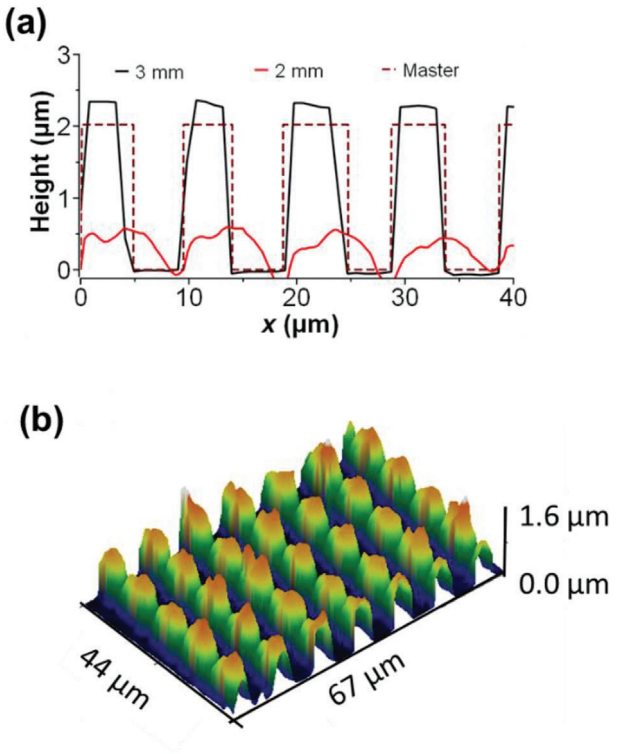

Figure 7. a) Height profiles of 5 µm pillars obtained from the part thicknesses of 3 and 2 mm on the *x*-direction (following the width of the stair). b) 3D confocal reconstruction of 5 µm pillars obtained with the 2 mm thickness stair and processing parameter set S_1.

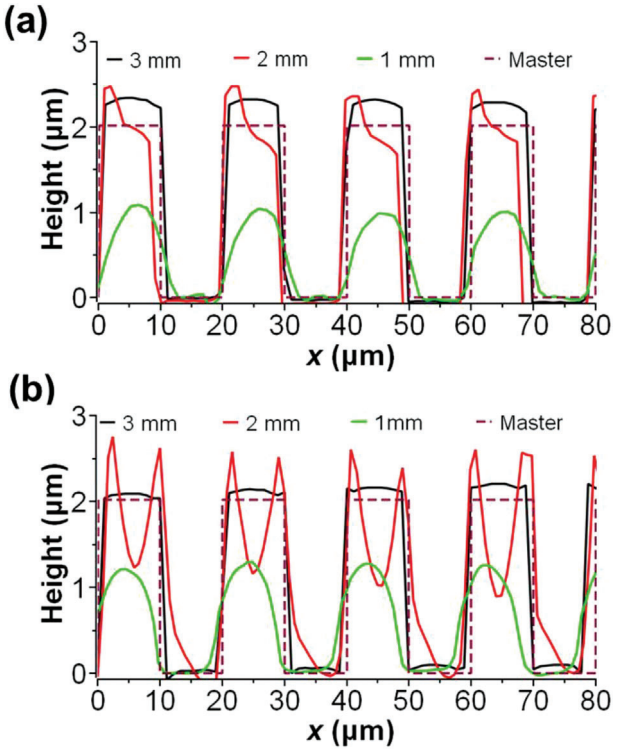

Figure 8. Height profile evolution for the 3.0, 2.0, and 1.0 part thicknesses of 10 µm lines a) and pillars b) in the *x*-direction (following the width of the stair) (parameter set S_2).

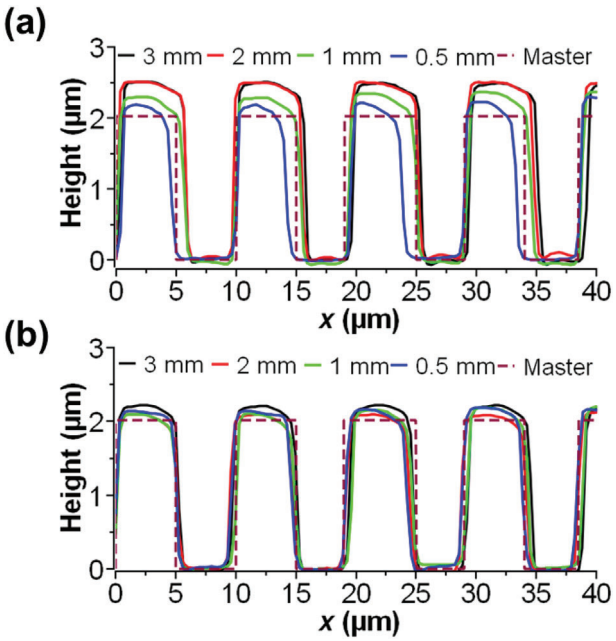

Figure 9. Height profile evolution for the 3.0, 2.0, 1.0, and 0.5 part thicknesses of 5 μm lines a) and pillars b) in the *x*-direction (following the width of the stair).

counteract the decrease in temperature, since if the curing is not sufficient during demolding, the textures can break.

In the case of parameters set S_3, a good replication was obtained for the pillars and lines analyzed. In the case of pillars (**Figure 9**a), a progressive loss of replication and deformation was observed for stairs 3 and 4 (e.g., thickness below 1 mm). In the case of lines (Figure 9b), replication was similar for all thicknesses.

The parameters set S_4 was tested to avoid the observed distortion in pillars replicated in the lower thickness. This parameters set consists of an increment of injection speed concerning parameters set S_3, which can favor filling the farthest areas. This change led to a good replication for all thicknesses, as shown in **Figure 10**.

Analyzing each texture (i.e., lines and pillars) separately, a different behavior was observed. Thus, *DOT* evolution for 5 μm pillars (Figure 10d) was characterized by the continuous increase of the replication height for the first three stairs, and a clear decrease for the fourth stair (i.e., a thickness of 0.5 mm). The effect was less pronounced for higher diameter sizes and line textures (i.e., no significant change was detected for different part thicknesses and microfeature sizes). Regarding height profiles, Figure 10b shows that the height of the replicated 5 μm pillar microfeatures regularly increased until a thickness of 0.5 mm was attained. In this case, the profile showed a clear deformation that provoked a decrease in the replication height. This effect was not seen for pillars with diameters higher than 5 μm nor, indeed, for any of the line textures (Figure 10a). In these cases, differences in *DOT* values (Figure 10c,d) and the part thickness were unclear, and only an oscillating trend was detected.

3.3. Mechanical Properties of Parts with Different Thicknesses

The stress-strain curves for specimens with different thicknesses obtained from the stairs mold are shown in **Figure 11**. They show a typical viscoelastic behavior.[34] Tensile properties are different for each thickness, i.e., the fracture strain increases with the thickness, whereas the elastic modulus progressively decreases (see **Table 3**). Such differences may be explained by considering the vulcanization process. With the aim of minimizing the cycle time, the specimens are extracted from the mold when they are rigid enough, even if the vulcanization process is not completed. This means that the grade of vulcanization would be higher in thinner specimens than in thicker ones. To rationalize this behavior, the vulcanization grade is estimated from the degree of crosslinking (n). Table 3 shows the degree of crosslinking calculated using equation 2. As expected, the degree of crosslinking decreases with thickness, which is consistent with the reduction of the elastic modulus and the increase in the fracture strain for thicker specimens. A post-curing process of the pieces would be necessary to homogenize the vulcanization degree and then obtain similar stress-strain behavior. The difference in viscoelastic behavior can be used to understand the changes in deformation depending on the thickness of the part. The elastic recovery after deformation depends on the elastic modulus, i.e., the higher the elastic modulus, the shorter the elastic strain, to the detriment of larger plastic deformation.

During the demolding step, the same deformation (stress) in microtextures is induced, regardless of part thickness. Thus, elastic recovery will be higher for thicker specimens, which means that the dimensional differences in the replica will be lower. Such differences in elastic properties explain the results obtained in Section 3.2. For thicker parts (3.0 mm), the geometry of the pillars results in less deformation. For lower thickness, deformation increases due to a shorter elastic recovery. This observation fits with the results obtained (Figure 10); the decrease in part thickness results in a progressive increase in deformation due to the different elastic properties of the part (i.e., elastic recovery decreases).

3.4. Surface Roughness

Roughness parameters were measured for the variety of the replicated microtextures. **Figure 12** shows the evolution of the values for the R_q parameters depending on the diameter and the geometry (more roughness parameters are presented in Section S1 in Supporting Information). The roughness obtained for each geometry within the same diameter is very close to each other. This similarity between the values is because, for the same diameter, the periodicities and the heights of the replicated textures are similar, giving rise to slight variations that the deviations can explain in the measurements. Comparing the diameters, it is possible to see a trend in the textures presented in the micro standard stamp (i.e., 5, 10, and 50 μm), decreasing the diameter the roughness increases. Smaller diameters have more textures in the same space due to their smaller periodicity, which increases roughness. It is not the case for 2 μm, whose dimensions of height and periodicity are different from the previous ones and differ for the trend.

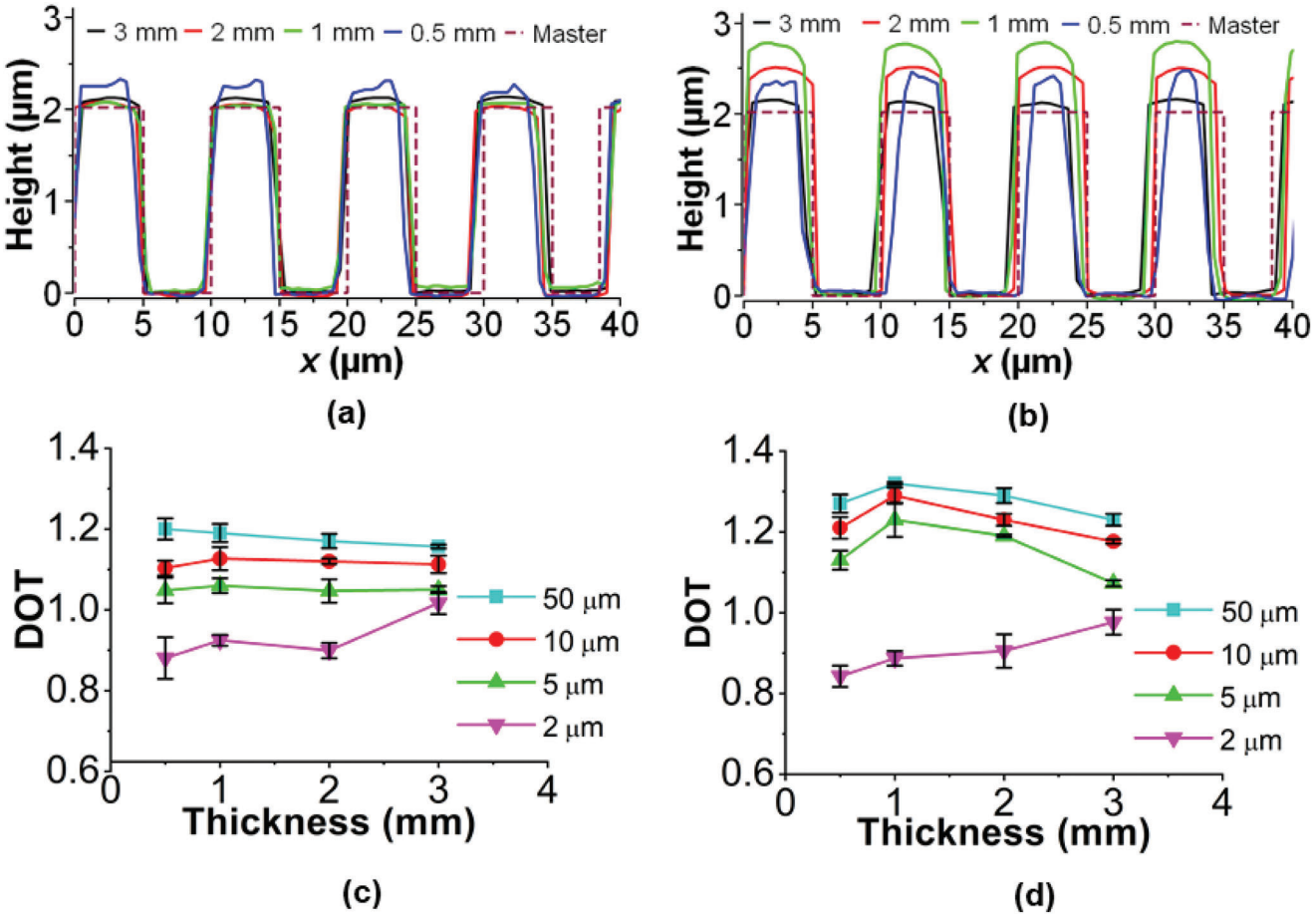

Figure 10. Height profile evolution for the 3.0, 2.0, 1.0, and 0.5 part thicknesses 5 μm lines a) and pilars b) in the *x*-direction (following the width of the stair). *DOT* (relation between the height of replication and the height of the master) evolution for c) lines and d) pillars textures with different size/diameter of microtextures.

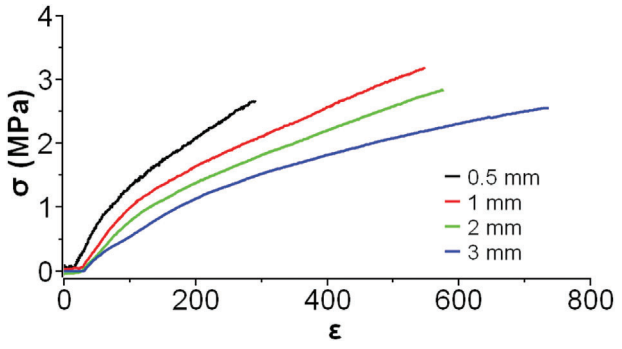

Figure 11. Experimental stress-strain curves obtained for specimen with different thickness.

Table 3. Results of elastic modulus and fracture strain (obtained from curves in Figure 11) and the degree of crosslinking (obtained from Equation (2)) for specimens with different thickness.

Thickness [mm]	Elastic modulus, *E* [MPa]	Fracture Strain [MPa]	Degree of crosslink, *n* [mol m^{-3}]
0.5	1.70±0.20	2.9±0.2	233±26
1.0	1.37±0.06	3.0±0.2	187±8
2.0	1.14±0.03	2.9±0.1	156±4
3.0	0.59±0.06	2.3±0.3	80±8

3.5. Surface Wettability

Contact angle (θ_c) values were measured for the different available textures and diameters (**Figure 13**). Results indicated that the θ_c could be increased up to 35° (vertical lines 2 μm) with respect to the value attained with a smooth surface. The θ_c variations obtained were consistent with the results published in the previous replication works. Depending on the geometries of the textures, increments of θ_c between 20° and 50° with respect to the smooth surface have been found.[21] Interestingly, different behaviors were found depending on the texture. Thus, the higher θ_c was obtained for the textures based on vertical lines and pillars. In both cases, the θ_c tended to increase as the diameter and the separation between microfeatures decreased, with the exception of sizes smaller than 2 μm. In all probability, the lower sizes were not ideal for measurement. However, despite the absence

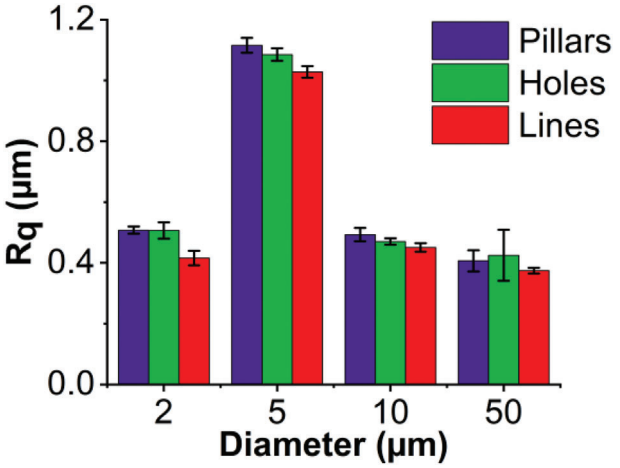

Figure 12. R_q values measured for the experimental samples obtained for the different textures and diameters.

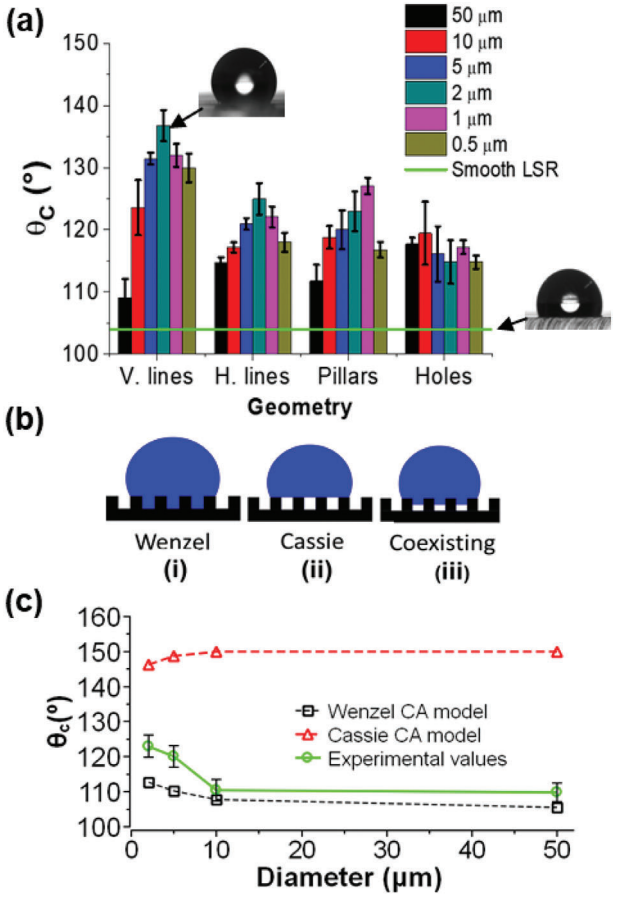

Figure 13. a) Dependence of the θ_c with the diameter/size of microfeatures for the different textures. b) Schemes of: Wenzel (i), Cassie- Baxter (ii) and coexisting (iii) models. c) Comparison between experimental and theoretical values of θ_c (calculated with Equations (S2.1-S2.4) for pillars with diameters between 2 and 50 μm).

of homogeneity and poor replication, the values of θ_c were still higher than those obtained with the smooth surface. The hole texture showed the minimum increase in the θ_c (i.e., from 104° to 114°) and a minimum repercussion on the specific diameter of the holes.

Is it well known that the texture of a surface has a marked influence on the θ_c that forms with a water drop, since this angle increases with the surface roughness.[35,36] Two different models have been suggested to explain the influence of textures. The Wenzel model[37] presumes a uniform interface between the textured surface and the water drop (**Figure 13**b-ii), whereas, in the Cassie Baxter model,[38] a complex solid-water-air interface exists (Figure 13b-ii). In this case, water drops remain on the top of the textured surface, leaving an intermediate air pocket. In real surfaces, Wenzel and Cassie Baxter models coexist (Figure 13b-iii). The formation of the air pockets experimentally depends on the geometry, spacing and diameter of textures, as seen in the different values obtained in the present work.

Figure 13c shows the results obtained for Wenzel and Cassie Baxter models for pillars compared with the experimental values. The process and equations to calculate the theoretical values was described in Section S2 (Supporting information).[39] Both extreme approximations proportionate different values for the microtextures that become lower (Wenzel model) and higher (Cassie model) than the experimental one. The best approximation was obtained using the coexisting model and the presence of air pockets between the microstructures. Therefore, the θ_c value depends on the surface roughness and the fraction area of the solid surface (i.e., the height of the air pockets). The results obtained for pillars with higher diameters (10 and 50 μm) are closer to the Wenzel model (i.e., smaller height pockets). By reducing the diameter and the separation between pillars (2 and 5 μm), the experimental values differ more from the Wenzel model (i.e., the influence and size of the air pockets increases).[40,41] It is interesting to remark that the higher increment in contact angle is for 2 μm ($R_q = 0.42 \pm 0.02$) lines with lower R_q value than 5 μm lines ($R_q = 1.03 \pm 0.02$). This roughness comparison shows that these smaller textures differ from the Wenzel model since the surface roughness and the formation of the air pockets influences the final θ_c value.

Horizontal lines showed the dependence between the increase of the θ_c and the decrease of the width. However, the difference found with the measurements attained with the vertical line texture should be noted, despite having the same geometry. The influence of the line orientation on the θ_c measurement is explained in **Figure 14**. Note (Figure 14a) that the θ_c can be differentiated in the $\theta_\perp$ and $\theta_{//}$ values depending on the orientation of texture lines (i.e., perpendicular and parallel angles for vertical and horizontal lines, respectively).[42] Figure 14b shows the differences between the contact angle orientations for each texture and diameters. It is possible to see that holes and pillars show minor differences. These slight differences for pillars and holes are expected because these structures have the same periodicity (i.e., the same roughness) in each orientation. For the lines, the periodicity depends on the orientation, and the effect is highly significant. Moreover, these differences depend on the diameter of the lines; the difference between the horizontal and perpendicular orientation increases for decreasing the diameters. This dependence can be explained because by reducing the width, the

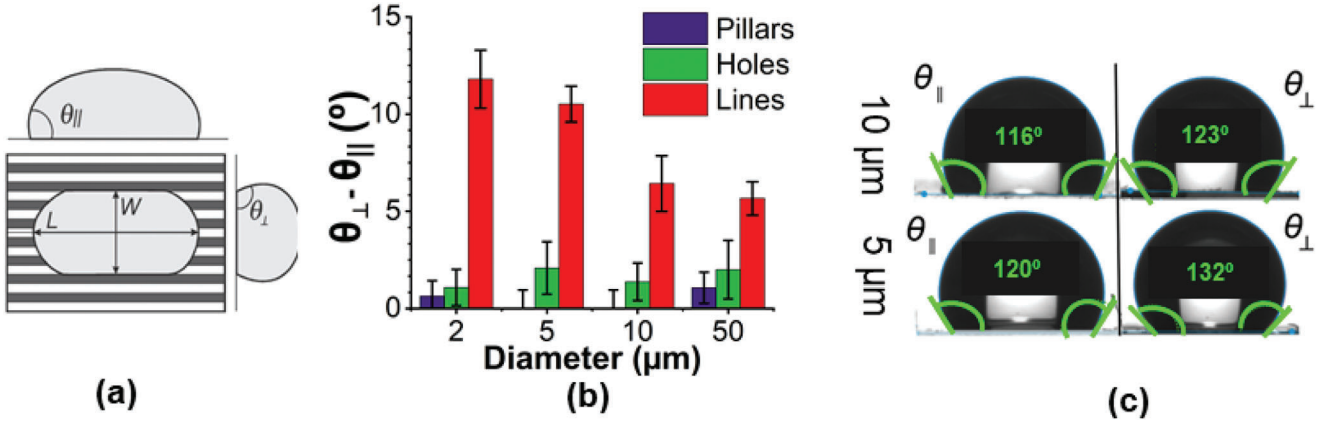

Figure 14. a) Scheme showing drops oriented parallel and perpendicular to the lines of the textured surface (reproduced under the Creative Commons Attribution 4.0 International License).[42] b) Comparison of the differences between contact angle measurements orientations for the different textures and diameters. c) Visual comparison between drops deposited on textures formed by horizontal lines ($\theta_{||}$) and vertical lines ($\theta_{\perp}$) of 10 and 5 μm width.

differences between the surface roughness of both orientations increase (i.e., lower diameters correspond to higher roughness) and lead to higher differences in contact angle measurements. Visual comparison between drop shapes for both orientations of lines of 5 and 10 μm is presented in Figure 14c; this difference is more pronounced for 5 μm.

Due to the interesting control of wettability and roughness, together with the higher productivity of the injection method, different applications in the medical field are being investigated (e.g., inhibition of bacterial adhesion and cell growth onto these news texture surface will be studied).

3.6. Durability of Textured Polymeric Films

Textured polymeric films obtained through the NIL replication technique have been used in at least ten cycles during the injection process. No difference in replication accuracy has been observed between successive injection cycles. Accordingly, the demolding step is good since there are no significant changes in height due to the residues of the replications that remain adhered to the texture in the film (**Figure 15**). Although the film has a durability of ten cycles, this translates into at least one order of magnitude in the lifetime of silicon master. However, in future work, it will be necessary to improve the durability of films, as some textured regions were prematurely broken as a consequence of wrinkles in the substrate or poor adhesion. Furthermore, the mold temperature at which a film may work under these conditions cannot exceed 160°C. Above this temperature, the adherence of the resin is lost, and it makes replication difficult. Different thermal post-curing of the UV resin and coatings are under study.

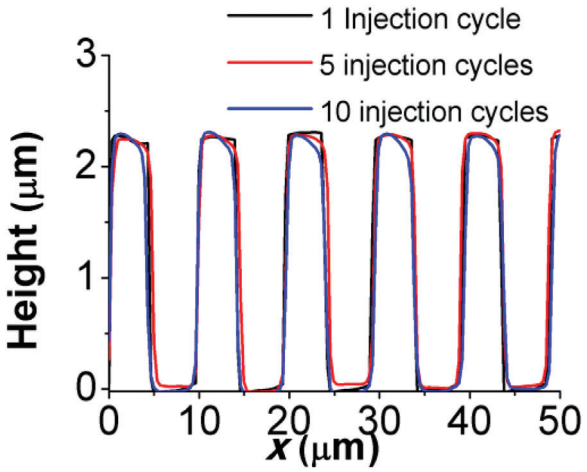

Figure 15. 5 μm pillars profiles in the *x*- direction (following the width of the stair) for 1, 5, and 10 injection cycles using the same film as a template.

4. Conclusion

It has been demonstrated that textured plastic foils replicated by NIL techniques can be effectively used as a template for replication with LSR injection techniques. Promising results have been obtained in the replication of textures having different types of microfeatures and sizes. According to all these points, the most relevant conclusions that may be drawn from the present work are:

i) The most affecting injection parameters for replication in a standard part were evaluated. Injection speed, curing time and mold temperature should be considered simultaneously when optimizing the process to improve replication. Increasing injection speed improves the replication and homogeneity of textures of small diameters. Moreover, reduction of the mold temperature allows greater fluidity for a longer period and longer paths into the mold, resulting in an improvement of replication. However, lower mold temperatures require a longer curing time. It is necessary to select a mold temperature that gives a good replication but without an excessively long curing time. Insufficient cure times can cause breakage of the textures during the demolding step.

ii) Textured areas at different distances from the injection point have been well-replicated by increasing the injection speed with respect to normal injection conditions. Furthermore, the zones away from the injection point provide less wear

in the textured areas of the film, improving the durability of the textured regions in the plastic films.

iii) Replication of the textures in regions with thicknesses between 3.0 and 0.5 mm has also been achieved. It has been shown that the mold temperature should be lowered to improve the filling of the thinner specimens. Differences in the vulcanization grade of the different thicknesses cause deformation of the microtextures in the demolding step. The deformation increases as the thickness decreases since the elastic recovery of the parts becomes smaller.

iv) The geometry, diameter, and separation between microfeatures influenced the θ_c values. Vertical lines and pillars with low diameters present better results than horizontal lines and holes. Furthermore, by measuring the θ_c in vertical and horizontal lines, it has been shown that its value varies depending on the orientation of the lines.

Supporting Information

Supporting Information is available from the Wiley Online Library or from the author.

Acknowledgements

This work was financially supported by the Catalonian Government through the funding grant ACCIÓ-Eurecat. N.L.-H. is a research fellow at Eurecat's "Vicente López" Ph.D. grant program. L.J.d.V. and J.P. acknowledge the financial support by Spanish Ministry of Economy and Competitiveness (Project MAT2018-(RTI2018-101827-B-100) and Generalitat de Catalunya (grant 2017SGR373).

Conflict of Interest

The authors declare no conflict of interest.

Data Availability Statement

The data that support the findings of this study are available from the corresponding author upon reasonable request.

Keywords

injection molding, microtextures, polymeric inlays, silicone rubber, wettability

Received: October 6, 2021
Revised: November 23, 2021
Published online:

[1] B. Bhushan, *Philos. Trans. R. Soc., A* **2009**, *367*, 1445.
[2] E. Mele, S. Girardo, D. Pisignano, *Langmuir* **2012**, *28*, 5312.
[3] T. Heckenthaler, S. Sadhujan, Y. Morgenstern, P. Natarajan, M. Bashouti, Y. Kaufman, *Langmuir* **2019**, *35*, 15526.
[4] J. Zhang, A. Rosenkranz, J. Zhang, J. Guo, X. Li, X. Chen, J. Xiao, J. Xu, *Int. J. Precis. Eng. Manuf. Technol.* **2021**, (Early Access): https://doi.org/10.1007/s40684-021-00358-z.
[5] W. R. Hansen, K. Autumn, *Proc. Natl. Acad. Sci. USA* **2005**, *102*, 385.
[6] P. G. Grützmacher, F. J. Profito, A. Rosenkranz, *Lubricants* **2019**, 7, 95.
[7] J. Voyer, Y.u Jiang, T. A. Pakkanen, A. Diem, *Polym. Test.* **2019**, *73*, 258.
[8] Y. Zheng, X. Gao, L. Jiang, *Soft Matter* **2007**, *3*, 178.
[9] A. Malshe, K. Rajurkar, A. Samant, H. N. Hansen, S. Bapat, W. Jiang, *CIRP Ann. – Manuf. Technol.* **2013**, *62*, 607.
[10] A. J. O'lenick, *J. Surfactants Deterg.* **2000**, *3*, 229.
[11] S. C. Shit, P. Shah, *Natl. Acad. Sci. Lett.* **2013**, *36*, 355.
[12] M. Meier, V. Dubois, S. Seeger, *Appl. Surf. Sci.* **2018**, *459*, 505.
[13] G. Fu, W. O. Soboyejo, *Mater. Sci. Eng., C* **2009**, *29*, 2011.
[14] J. Li, M. Wang, Y. Shen, *Surf. Coat. Technol.* **2012**, *206*, 2161.
[15] G. R. J. Artus, S. Jung, J. Zimmermann, H.-P. Gautschi, K. Marquardt, S. Seeger, *Adv. Mater.* **2006**, *18*, 2758.
[16] L. Chen, X. Wang, T. Yang, H. Ping, P. Bennett, Z. Zheng, Q. Yang, W. Perrie, S. P. Edwardson, G. Dearden, D. Liu, *J. Phys. D: Appl. Phys.* **2018**, *51*, 445301.
[17] R. S. Haines, A. H. F. Wu, H. Zhang, J. Coffey, T. Huddle, J. S. Lafountaine, Z. Lim, E. A. White, N. T. Tuong, *J. Chem. Educ.* **2009**, *86*, 365.
[18] L. Phan, S. Yoon, M.-W. Moon, *Polymers (Basel)*. **2017**, *9*, 417.
[19] Z. Yan, X. Liang, H. Shen, Y. Liu, *IEEE Trans. Dielectr. Electr. Insul.* **2017**, *24*, 1743.
[20] Z. Yuan, J. Xiao, J. Zeng, C. Wang, J. Liu, S. Xing, D. Jiang, G. Du, F. Yang, C. Peng, H. Chen, Q. Ye, J. Tang, *Surf. Coat. Technol.* **2010**, *205*, 1947.
[21] C. Hopmann, C. Behmenburg, U. Recht, K. Zeuner, *Silicon* **2014**, *6*, 35.
[22] P.-E. Zhang, Y. Mischkot, M. Hansen, H. Hansen, Presented at Proc. 15th Int. Conf. Metrol. Prop. Eng. Surfaces, ASPE Am. Soc. Precis. Eng. Replication of microstructures on three-dimensional geometries by injection moulding of liquid silicone rubber, Charlotte NC, March, **2015**.
[23] J. M. Stormonth-Darling, N. Gadegaard, *Macromol. Mater. Eng.* **2012**, *297*, 1075.
[24] S. W. Park, W. I. Lee, S. N. Moon, Y.-E. Yoo, Y. H. Cho, *eXPRESS Polym. Lett.* **2011**, *5*, 950.
[25] H. Lan, Y. Ging, in *Lithography*, (Ed: M. Wang), Intech Open Limited, London, United Kingdom **2010**, Ch.23.
[26] L. J. Guo, *Adv. Mater.* **2007**, *19*, 495.
[27] A. F. Lasagni, C. Gachot, K. E. Trinh, M. Hans, A. Rosenkranz, S. Eckhardt, T. Kunze, M. Bieda, D. Günther, V. Lang, in *Proc. Laser-Based Micro- Nanoprocessing XI*, SPIE, Bellingham, WA **2017**, p. 10092.
[28] A. Rosenkranz, M. Hans, C. Gachot, A. Thome, S. Bonk, *Lubricants* **2016**, 4, 2.
[29] H. Schift, C. Spreu, M. Saidani, M. Bednarzik, J. Gobrecht, A. Klukowska, F. Reuther, G. Gruetzner, H. H. Solak, *J. Vac. Sci. Technol., B: Microelectron. Nanometer. Struct.– Process., Meas., Phenom.* **2009**, *27*, 2846.
[30] Y. Chen, *Microelectron. Eng.* **2015**, *135*, 57.
[31] H. J. Lim, J. J. Lee, S. Park, K.-B. Choi, G. H. Kim, H. H.a Park, J.i H. Ryu, *J. Nanosci. Nanotechnol.* **2012**, *12*, 5489.
[32] Y.-H. Zang, R. Muller, D. Froelich, *Polymer (Guildf)* **1989**, *30*, 2060.
[33] J. Schweitzer, S. Merad, G. Schrodj, F. Bally-Le Gall, L. Vonna, *J. Chem. Educ.* **2019**, *96*, 1472.
[34] A. M. Stricher, R. G. Rinaldi, C. Barrès, F. Ganachaud, L. Chazeau, *RSC Adv.* **2015**, *5*, 53713.
[35] H. Teisala, H.-J. Butt, *Langmuir* **2019**, *35*, 10689.
[36] K. Y. Law, H. Zhao, *Surface Wetting: Characterization, Contact Angle, and Fundamentals*, Springer, New York **2015**.
[37] R. N. Wenzel, *Ind. Eng. Chem.* **1936**, *28*, 988.
[38] A. B. D. Cassie, S. Baxter, *Trans. Faraday Soc.* **1944**, *40*, 546.
[39] E. Puukilainen, T. Rasilainen, M. Suvanto, T. A. Pakkanen, *Langmuir* **2007**, *23*, 7263.
[40] J. Bico, U. Thiele, D. Quéré, *Colloids Surf., A* **2002**, *206*, 41.
[41] X. J. Feng, L. Jiang, *Adv. Mater.* **2006**, *18*, 3063.
[42] J. J. Faria-Briceno, A. Neumann, P. R. Schunk, S. R. J. Brueck, *Sci. Rep.* **2019**, 9, 5723.

